Wind Energy

WIND ENERGY
Wind Energ. 2015; **18**:1685–1702
Published online 14 July 2014 in Wiley Online Library (wileyonlinelibrary.com). DOI: 10.1002/we.1781

RESEARCH ARTICLE

The dynamics of an offshore wind turbine in parked conditions: a comparison between simulations and measurements

Rasoul Shirzadeh, Wout Weijtjens, Patrick Guillaume and Christof Devriendt

Acoustics and Vibration Research Group (AVRG), Department of Mechanical Engineering, Vrije Universiteit Brussel (VUB), Pleinlaan 2, B-1050 Brussels, Belgium

ABSTRACT

Offshore wind turbines are complex structures, and their dynamics can vary significantly because of changes in operating conditions, e.g., rotor-speed, pitch angle or changes in the ambient conditions, e.g., wind speed, wave height or wave period. Especially in parked conditions, with reduced aerodynamic damping forces, the response due to wave actions with wave frequencies close to the first structural resonance frequencies can be high. Therefore, this paper will present numerical simulations using the HAWC2 code to study an offshore wind turbine in parked conditions. The model has been created according to best practice and current standards based on the design of an existing Vestas V90 offshore wind turbine on a monopile foundation in the Belgian North Sea. The damping value of the model's first fore-aft mode has been tuned on the basis of measurements obtained from a long-term ambient monitoring campaign on the same wind turbine. Using the updated model of the offshore wind turbine, the paper will present some of the effects of the different design parameters and the different ambient conditions on the dynamics of an offshore wind turbine. The results from the simulations will be compared with the processed data obtained from the real measurements. The accuracy of the model will be discussed in terms of resonance frequencies, mode shapes, damping value and acceleration levels, and the limitations of the simulations in modeling of an offshore wind turbine will be addressed. Copyright © 2014 John Wiley & Sons, Ltd.

KEYWORDS
offshore wind turbine; simulations; measurements; parked conditions; dynamics; damping

Correspondence
R. Shirzadeh, Acoustics and Vibration Research Group (AVRG), Department of Mechanical Engineering, Vrije Universiteit Brussel (VUB), Pleinlaan 2, B-1050 Brussels, Belgium.
E-mail: rshirzad@vub.ac.be

Received 19 March 2013; Revised 25 April 2014; Accepted 6 June 2014

1. INTRODUCTION

The size of commercial wind turbines has increased dramatically in the last 25 years from approximately a rated power of 50 kW and a rotor diameter of 10–15 m up to today's commercially available 5 MW machines with a rotor diameter of over 120 m. A total of 418 new offshore wind turbines, in 13 wind farms, were fully grid connected during 2013. This makes a total of 1567 MW, which is 34% more than installed wind turbines in 2012.[1] All in all, the offshore installed wind capacity is currently near 6.5 GW, including 2080 turbines in 69 wind farms in 11 European countries. A forecast of 9.4 GW installed in Europe by the end of 2014 seems realistic, taking into account the projects already under construction.[2] Regarding long-term forecasts for the offshore wind industry, investment and employment in the offshore wind power business are expected to grow considerably and continuously at least until 2030.[3]

Many large-scale offshore wind farm projects use monopile foundations to obtain a cost effective design. During the design of these monopile structures, fatigue due to combined wind and wave loading is one of the most important problems to take into account. Coincidence of structural resonances with those dynamic wind and wave forces can lead to large stresses and subsequent accelerated fatigue. Coupling between wave-induced motion and turbine motion is expected to be significant and has to be taken into account during design analysis.[4]

Damping ratios are crucial for lifetime predictions as the amplitude of vibrations at resonance are inversely proportional to these ratios. The overall damping of the first bending mode of an offshore wind turbine consists of a combination of aerodynamic damping and damping due to active/passive devices, such as a tuned mass damper (TMD), and additional offshore damping, e.g., structural damping.[5,6] Compared with onshore support structures, the additional damping is further influenced by effects such as soil damping and hydrodynamic damping. Real damping ratios are difficult to predict by numerical tools, and therefore, measurements on existing offshore wind turbines are crucial to verify existing design assumptions.[7] Several measurement studies have previously been performed at different offshore wind farms. The most of the offshore research is focused on the wake effects. Torben J. Larsen *et al.*[8] have investigated wake effects on load and power production by using the dynamic wake meander model implemented in HAWC2 for a wind turbine located in Dutch Egmond aan Zee wind farm.

A limited number of offshore measurements deals with the dynamic behavior of the wind turbines. Damgaard *et al.*[9] performed 'rotor-stop' tests for five wind parks for the period between 2006 and 2011 and determined the natural frequency and modal soil damping of a specific wind turbine for different soil conditions. Häckell[10] has extracted the modal parameters for an offshore wind turbine on a tripod structure located at the German Alpha ventus wind farm. Ozbek and Rixen[11] has reported the results for an onshore 2.5 MW wind turbine at both standstill and rotating conditions by using three different measurement systems, namely conventional strain gages, photogrammetry and laser interferometry. Devriendt *et al.*[12] performed an overspeed stop test to estimate the overall damping of the first FA mode of a V90 wind turbine in the Belgian Belwind wind farm. Devriendt *et al.*[13] discussed the results of the 2 weeks monitoring period while the same wind turbine was in parked conditions. He presented the resonance frequencies and damping values of the most dominant modes identified during this monitoring period. Recently, Shirzadeh *et al.*[14] have evaluated the contribution of every source of damping, e.g., aerodynamic damping, hydrodynamic damping, soil and structural damping, from both simulations and measurements. However, a few investigations have been reported for measurements on a standstill (parked) offshore wind turbine. This calls for a detailed research in the area, which is described in this paper.

This paper does not focus on the theoretical background of the utilized algorithms but on the application of these methods on measured and simulated data for an offshore wind turbine. The paper is structured as follows. First, the utilized measurement system is summarized. The main features of the aeroelastic simulations of the offshore wind turbine, implemented in HAWC2, are then described. We will recapitulate some of the results in order to compare them with the simulations. The measurements are obtained during a measurement campaign on an offshore wind turbine in the Belgian North Sea. These results have been presented at two European Wind Energy Association conferences and are discussed in detail in the works by Devriendt *et al.*[12,13] Using the simulation model of the offshore wind turbine the paper will end with illustrating and explaining some of the effects of the different ambient conditions, e.g., changing tidal level, wave height, wave period and wind speed on the dynamics of an offshore wind turbine in parked conditions. The simulated natural frequencies, damping values and acceleration levels will be compared with those obtained from the measurements. The paper will discuss the accuracy of the results and the limitations of the used simulations in modeling an offshore wind turbine according to best practice and current standards and using state-of-the art modeling software.

2. OFFSHORE MEASUREMENTS

Within the OWI-project (www.owi-lab.be), a long-term monitoring camping is ongoing at the Belwind wind farm, which consists of 55 Vestas V90 3 MW wind turbines. The wind farm is located in the North Sea on the Bligh Bank, 46 km off the Belgian coast (Figure 1).

The hub-height of the wind turbine is on average 72 m above the lowest astronomical tide (LAT). Each transition piece (TP) is 22 m high and has a weight of 167 t. The tests are performed on the BBC01-turbine that is located in the north of the wind farm directly next to the offshore high voltage substation. The wind turbine is placed on a monopile foundation structure with a diameter of 5 m and a wall-thickness of 6 cm. The actual water depth at the location of BBC01 is 24.03 m with respect to LAT, and the monopile has a penetration depth of 20.9 m from the mudline. The soil is considered as stiff and mainly consists of sand. Figure 2 shows the soil profiles and properties for every layer, which is in accordance with the data from the Belwind wind farm at the location of the monitored wind turbine.

The structures instrumented in this campaign were the tower and the TP. Measurements were taken at four levels on nine locations using a total of 10 sensors. The measurement locations are indicated in Figure 1 by yellow circles. The locations are chosen on the basis of the convenience of sensor mounting, such as the vicinity to the platforms. The chosen levels are 69, 41, 27 and 19 m above LAT, respectively, level 1 to 4. There are two accelerometers mounted at the lower three levels and four at the top-level. The chosen configuration is primarily aimed at the identification of tower bending modes. The two extra sensors on the top-level are placed to capture the tower tor-

Wind Energ. 2015; **18**:1685–1702 © 2014 John Wiley & Sons, Ltd.
DOI: 10.1002/we

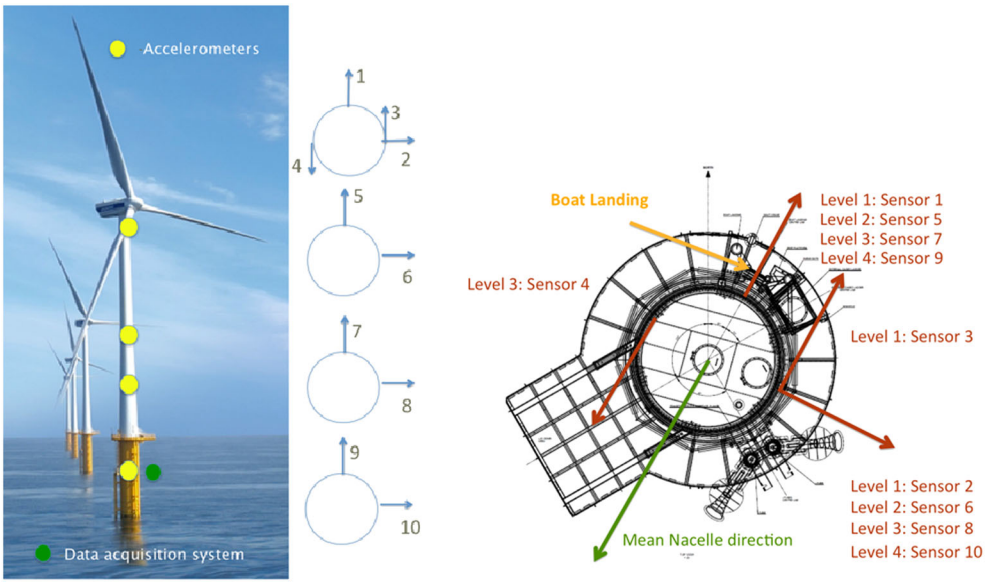

Figure 1. Offshore V90 wind turbine (left) measurement locations on BBC01 (right).

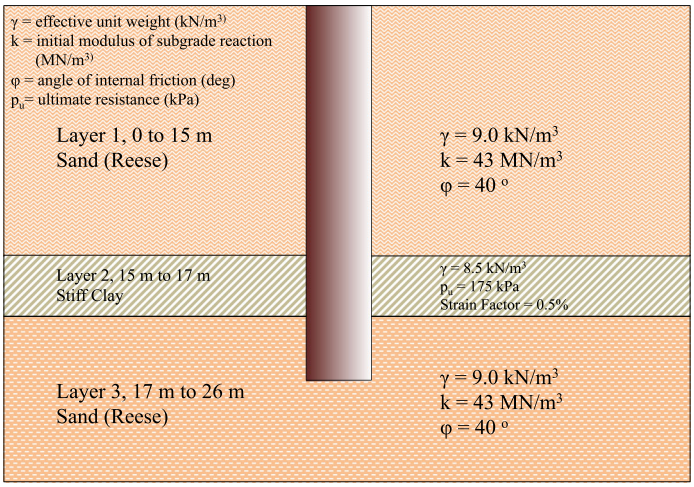

Figure 2. Different soil profiles for the monopile support at wind turbine location.

sion. The data acquisition measures continuously and sends data every 10 min to the server that is located onshore. The description of the measurement set up and used analysis-techniques have been discussed in detail by Devriendt *et al.*[12,13]

In this paper, we will focus on the data-set obtained while the wind turbine was in standstill or in parked condition. During this monitoring campaign, the mass-tuned damper was always active. In Figure 3, the corresponding SCADA data for the monitoring period is given. Each point in the plots corresponds to the data with a time interval of 10 min. Therefore, the plots represent the results for 2 weeks of parked conditions. The wind speed varies between 0 and 18 ms^{-1}. The pitch angle is almost constant during the period of analysis, with a pitch angle of 78° or 88.3°. Most of the times, the wind turbine is idling with a speed lower than 1.3 rpm, and sometimes, the wind turbine was in parked conditions. Both conditions allow us to sufficiently comply with the time-invariant Operational Modal Analysis (OMA) assumptions and avoid the presence of harmonic components in the frequency range of interest.[12] During the parked conditions, the wind turbines are actively yawed. This assures that the nacelle direction is always aligned with the mean wind direction.

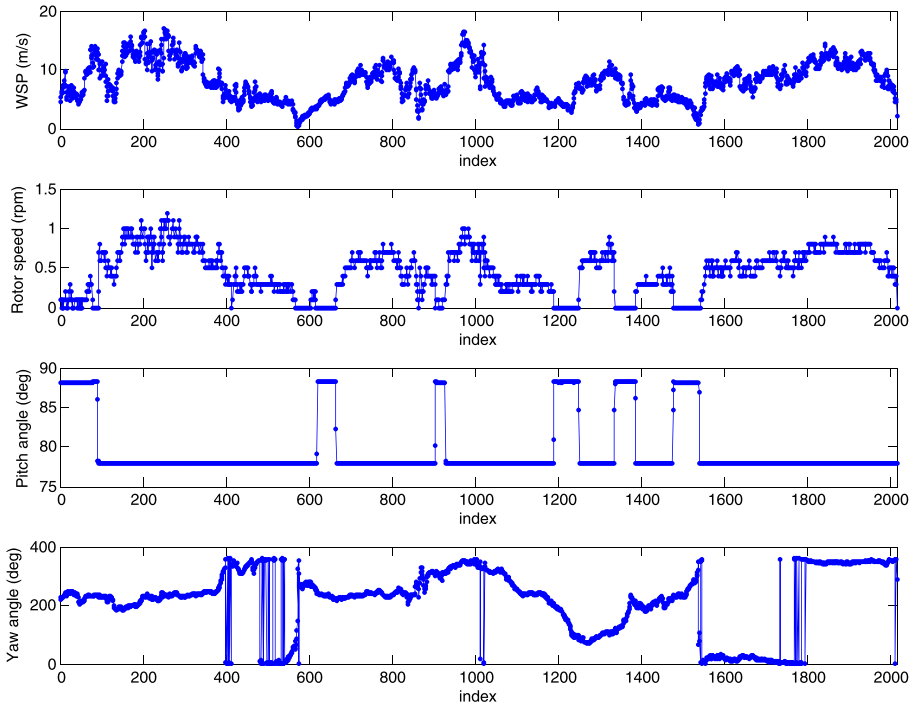

Figure 3. SCADA data for monitoring period from top to down: wind speed, rotor speed, blades pitch angle and yaw angle.

3. THE HAWC2 MODEL

The numerical simulations have been carried out using HAWC2 aeroelastic code developed at DTU. HAWC2 uses a multibody formulation, allowing the user to model each component of the turbine as a separate body. The implementation of each body is carried out adopting finite element theory. The code is capable of simulating the structural response of a pitch-controlled horizontal axis wind turbine subject to aerodynamic, hydrodynamic and soil loads.

The detailed specifications of the blade aerodynamic properties, monopile foundation, tower, nacelle and drivetrain structural properties, are provided as an input file for the HAWC2 code. The hydrodynamic and elastic properties of the offshore support are also collected. A comprehensive description on the wind turbine components is available in the work by Shirzadeh *et al.*[14]

3.1. Aerodynamic model

The aerodynamic model in HAWC2 is based on the blade element momentum theory, which is extended with models to handle the dynamic inflow, skew inflow, shear effect on induction, effect from large blade deflections and tip loss. Also, the modified Beddoes–Leishman model is used, which models the dynamic stall in the numerical model.

It is possible to model both deterministic and stochastic wind in HAWC2. The deterministic part of the wind includes mean wind velocity, sudden acceleration, linear trend, special gust events and special shears. The stochastic wind is usually referred to as turbulent wind. Stochastic wind is achieved by simulating atmospheric turbulence using Mann's turbulence model with a Kaimal spectrum. The length of the turbulence box is selected in such a way that is sufficient for the highest used wind speed (20 ms^{-1}). There are 32,768 sheets of 64 by 64 points. Therefore, the longitudinal resolution of the turbulence box is 2.3 m, which is considered as a fine resolution comparing with other reported turbulence boxes.[15] The lateral and vertical resolutions of the box are 2 and 3 m, respectively. The simulations are carried out for 50 min, and the first 10 min segment is removed to avoid the transient behavior at the beginning of the simulations. The turbulence intensity is dependant on the wind speed and is extracted from the Belwind measurements at hub height and set as a parameter in HAWC2. According to the measurements performed at Belwind, the wind speed has a power profile with $\alpha = 0.11$. Furthermore, the tower shadow effects, which account for the wind condition changes near the tower, are used in simulations.

Wind Energ. 2015; **18**:1685–1702 © 2014 John Wiley & Sons, Ltd.
DOI: 10.1002/we

3.2. Hydrodynamic model

The hydrodynamic loads in HAWC2 are calculated on the basis of Morrison's equation. Morrison's equation is the sum of two force components: an inertia force in phase with the local flow acceleration and a drag force proportional to the square of the instantaneous flow velocity. According to Veldkamp and Van Der Tempel,[16] the inertia component is dominant for offshore wind turbine support structures with the currently characteristic diameter of 3–5 m in intermediate water depths of 5–25 m. Several empirical calculation methods exist to find the appropriate inertia (C_m) and drag (C_d) coefficients. For random wave fields used in fatigue calculations, the design rules advise, for a vertical cylinder following coefficients, $C_m = 2.0$ and $C_d = 0.65$.[17] The Christchurch Bay experiments,[18] which seem of particular relevance because they deal with random waves, concluded that for inertia-dominated load cases, the inertia coefficient approaches the value of 2.0. The drag coefficient could not be determined so accurately, but at least common values of $C_d = 0.65$ to 1.05 are not contradicted.

Note that the Morrison's equation is valid when the cylinder is small compared with the wave length ($D/L < 0.2$). For large diameter cylinders, such as the monopile in our model, the inertia force dominates and can be estimated by diffraction theory. For a large vertical cylinder, the solution is given by MacCamy–Fuchs.[19] On the other hand, HAWC2 does not consider diffraction effects internally. Therefore, applying an inertia coefficient of $C_m = 2.0$ cause the loads to be overestimated. If diffraction effect is considered (e.g., using the MacCamy–Fuchs correction), then the C_m coefficient would go down to around $C_m = 1$.

The appropriate C_m value is actually a function of water depth. By applying the diffraction theory,[19] the C_m coefficient versus water depth is listed in Table I. A constant value of 10 cm is assumed to account the marine growth along the monopile. Also, regarding the aforementioned discussions, a drag coefficient of $C_d = 1.0$ is selected in simulations.

The water kinematics describes how the sea condition is considered to influence the structure. The wave kinematics are provided through a defined dynamic link library interface, including both regular and irregular airy waves. For this study, an irregular airy wave model with JONSWAP[20] spectra has been used. The implementation of JONSWAP wave spectra in HAWC2 is carried out using three input parameters including the significant wave height H_s, peak period T_p and peak enhancement factor γ. The γ depends on the H_s/T_p ratio, and the relationship for this is suggested in the work of Veritas.[19] The corresponding γ is calculated for different wave heights and wave periods and the used in simulations.

3.3. Soil model

For the pile foundation, we used the distributed springs model. This model idealizes the monopile with a flexible foundation as a free-free beam with lateral (Winkler-type) springs distributed along the subsoil portion of the monopile. This provides a more realistic representation of the lateral stiffness along the monopile. The beam uses the real properties of the monopile both above and below the mudline. The spring stiffness of the subsoil portion is calculated on the basis of the *p-y* model and is depth-dependent.[21]

Soil models for sand and clay show a relatively simple nonlinear behavior. Such models are well described in certain standards,[22] and the derivation is not very complicated.[23] On the basis of the two soil properties, the effective unit weight (γ) and angle of internal friction (ϕ), together with the pile diameter, the API standard[22] describes a straightforward approach to derive the *p-y* curves over depth.

Layered soil conditions have been considered in order to achieve both realistic soil conditions and a certain participation of the resulting soil–structure interaction model in the dynamic response. The soil consists of three layers of sand and clay with different properties in terms of internal friction angles (Figure 2). The full pile foundation is modeled in LPILE

Table I. Inertia coefficient as a function of water depth for a monopile from mudline to surface.

Depth below LAT (m)	D	$D + D_{\text{marine}}$	D/L	C_m (MacCamy–Fuchs)
0.0	4.30	4.40	0.377	1.271
−1.0	4.30	4.40	0.377	1.271
−2.0	4.30	4.40	0.377	1.271
−4.0	4.00	4.10	0.352	1.367
−6.0	4.33	4.43	0.380	1.261
−8.0	4.67	4.77	0.409	1.162
−10.0	5.0	5.10	0.437	1.071
−15.0	5.0	5.10	0.437	1.071
−20.0	5.0	5.10	0.437	1.071
−26.03	5.0	5.10	0.437	1.071

software, a program for analyzing a pile under lateral loading, and the data including the *p-y* curves at a 1 m spacing along the length of the pile is provided as an input file in HAWC2 to model the soil. In this paper, we assume that the soil only exerts lateral forces. The axial forces and torsional moment are assumed to be negligible.

4. NATURAL FREQUENCIES AND MODE SHAPES

The natural frequencies of the structure were identified using automated operational modal analysis applied to the measurement data; details can be found in the works by Devriendt *et al*.[24] During an initial overspeed stop test, several natural frequencies were identified between 0 and 2 Hz. The long-term monitoring period is focused on five dominant modes. The identified modes from both the overspeed stop and long-term monitoring are listed in Table II. For the long-term monitoring, the standard deviation of the dominant frequencies is added.

Figure 4 presents the mode shapes of those five modes that were monitored during the monitoring period. The first mode is the first support structure FA bending mode (S1FA). The second mode is the first support structure SS bending mode (S1SS). These modes are characterized by a lot of motions at the nacelle level. Next, we identify a mode with a second FA bending mode behavior in the tower and almost no motion at the nacelle level (B1AEP). This mode corresponds, in fact, with a blade mode, as will be shown by the simulations. The last two modes are the second bending modes of the support structure in respectively the side-side (S2SS) and fore-aft (S2FA) directions. To characterize these modes correctly, we will now compare them with the modes obtained from the simulations.

The HAWC2 simulations consist of both eigenvalue and time domain simulations. First, an eigenvalue analysis has been performed to identify the natural frequencies of the offshore wind turbine in the parked condition. The blades are pitched to 78°. Table II compares the obtained frequencies from measurements and simulations for the first 10 lowest identified modes.

Figure 4 represents only those five mode shapes, which were also identified during the monitoring period. The measurements are not able to identify the blade modes as the sensors are mounted on the tower and TP. However, the simulations have this advantage to distinguish the blade modes from other modes and track them in measurements.

Additionally, a time domain simulation is performed for the wind turbine in parked condition with the same blade pitch angle. For this analysis, the ambient conditions were selected similar as those experienced during the overspeed test. The wind speed and the wind-wave misalignment were, respectively, 4.5 ms^{-1} and 20°. The selected significant wave height (H_s) and wave period (T_p) are, respectively, 0.5 m and 3.5 s. The simulation is carried out for 2600 s, and the first 200 s are discarded to avoid transient behavior at the beginning of the simulation. Figure 5 displays the time domain accelerations for three levels in FA direction. The time domain data can be analyzed in a similar way as for the measurements[25] using a state-of-the-art operational modal analysis technique, pLSCF. All stabilization diagrams (Figure 5) seem to have around four or five well identifiable stable poles. The identified frequencies are listed in Table II. To compare the mode shapes from simulations with those obtained from the measurements, one can compare the modal assurance criterion (MAC)[26] coefficient. The MAC evaluates the degree of correlation between two mode shapes over subsequent instants resulting in a value close to one for corresponding modes. The MAC values are calculated for the five dominant mode shapes and are shown in Table III.

We can conclude that the eigenfrequencies and mode shapes identified during the monitoring period compare well with the time domain simulations. The highest difference on both frequency and mode shape can be found for the blade mode (B1AEP). This can be explained by the fact that we did not use the real blade data but a downscaled version of the NREL 5 MW reference wind turbine. In the real measurements, we also found a slightly larger difference between the second

Table II. Experimental and computational natural frequency comparison for 10 lowest frequencies.

Description	Long-term measurements Mean freq±Std freq (Hz)	Overspeed stop test Freq (Hz)	HAWC2 (Eigenvalue analysis) Freq (Hz)	HAWC2 (Time domain) Freq (Hz)
First support structure FA (S1FA)	0.361 ± 0.004	0.353	0.374	0.366
First support structure SS (S1SS)	0.366 ± 0.004	0.363	0.380	0.371
First blade asymmetric flapwise pitch (B1AFP)	—	0.667	0.828	—
First blade asymmetric flapwise yaw (B1AFY)	—	0.753	0.850	—
First drivetrain torsion (DTT1)	—	1.071	1.028	—
First blade collective flap (B1CF)	—	1.152	1.144	—
First blade asymmetric edgewise pitch (B1AEP)	1.201 ± 0.005	1.200	1.145	1.098
First blade asymmetric edgewise yaw (B1AEY)	—	1.357	1.444	1.334
Second support structure SS (S2SS)	1.449 ± 0.018	1.466	1.662	1.428
Second support structure FA (S2FA)	1.560 ± 0.016	1.570	1.756	1.504

Wind Energ. 2015; **18**:1685–1702 © 2014 John Wiley & Sons, Ltd.
DOI: 10.1002/we

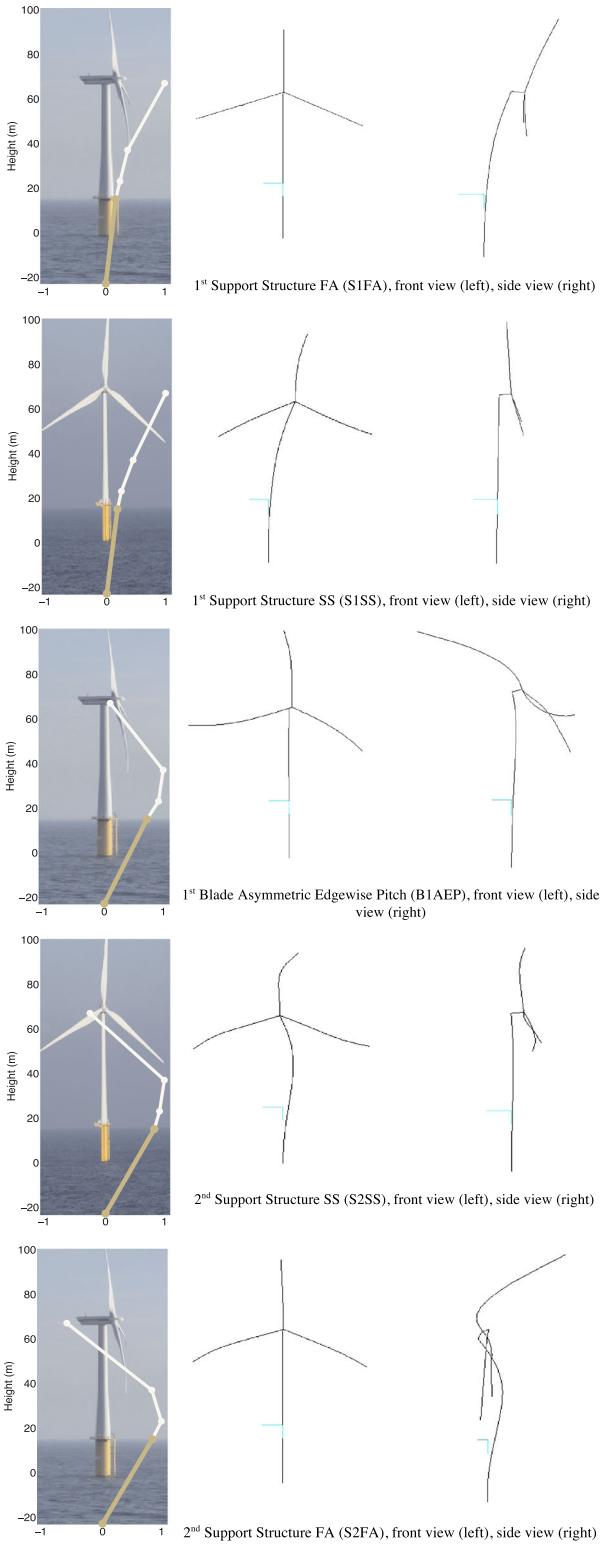

Figure 4. Mode shapes of the support structure for the five dominant frequencies from measurements (left) and HAWC2 eigenvalue analysis (right).

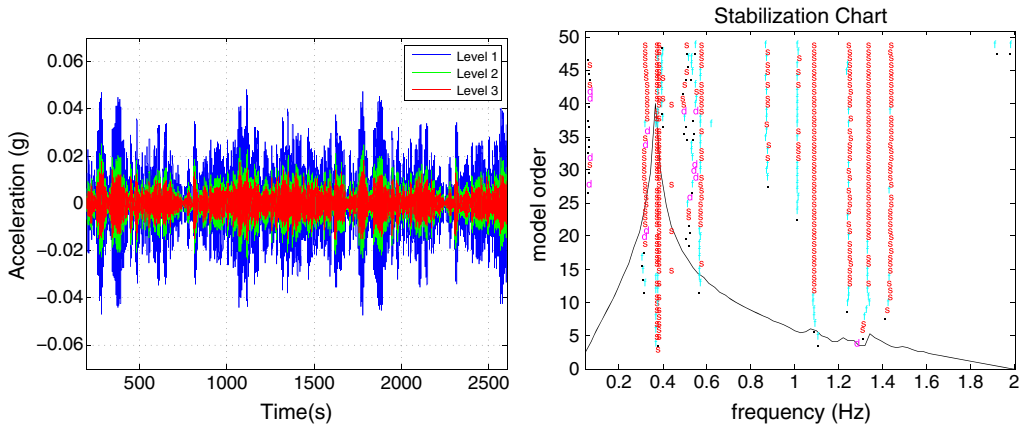

Figure 5. Estimated time domain signals in FA direction (left); stabilization diagram using the pLSCF method (right).

Table III. Comparing the mode shapes derived from the HAWC2 with the measured mode shapes.

Mode	MAC value	Mode	MAC value
S1FA	0.954	S2SS	0.984
S1SS	0.999	S2FA	0.924
B1AEP	0.777		

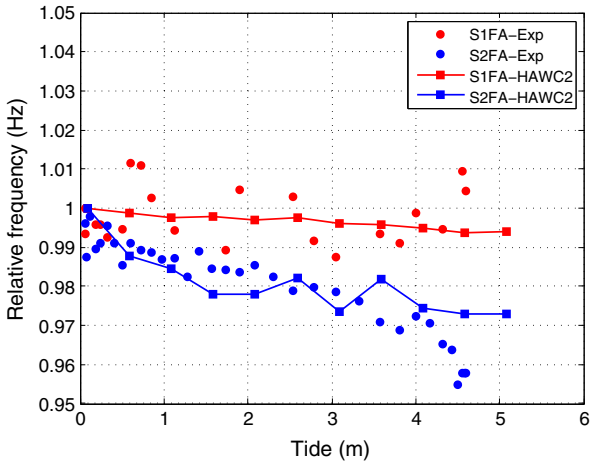

Figure 6. Relative resonance frequency comparison for the first FA and second SS modes as a function of tidal levels.

bending modes in the FA and SS directions than in the simulations. This is due to the soil stiffness which, in reality, might not be symmetrically distributed. Another reason might be the boat-landing and the J-tubes, which are not considered in HAWC2. These secondary steel structures might considerably alter the stiffness or frequencies of the second bending modes, considering the relative large displacements of these modes around the TP.

Comparing with the eigenvalue analysis, the time domain analysis results in lower frequencies. This is due to the hydrodynamic mass of the water, which is not taken into account in the eigenvalue analysis. The hydrodynamic loading appears as an additional mass to the system causing the frequencies to shift to a lower value. We also have observed this in the variation of the resonance frequencies in the measurements due to the tidal effect. The tidal levels at the Belwind wind farm show a maximum difference between the highest and LAT of approximately 4 m. Additional simulations have been executed for different water levels, and the dominant resonance frequencies are obtained to see the influence of sea level on the resonance frequencies.

Wind Energ. 2015; **18**:1685–1702 © 2014 John Wiley & Sons, Ltd.
DOI: 10.1002/we

Figure 6 presents the variation of the resonance frequencies in function of the tidal level. For higher sea levels, the natural frequencies decrease because the hydrodynamic added mass is increased. The first bending modes are less sensitive to this effect in comparison with the second bending modes. This can be explained by the fact that the second mode has relatively large displacements at the TP compared with the nacelle. In contrast, the first-order mode motion is greatest at the nacelle, and relatively little motion occurs at the TP. The variations in natural frequencies for different tides are shown for both simulations and measurements in Figure 6.

5. DAMPING VALUES OF THE FUNDAMENTAL FA AND SS MODES

In this section, the estimated damping values from measurements will be compared with the results of numerical simulations. The first part of this section discusses the tuning procedure of the damping in the numerical model. The tuned model is then used to investigate the influence of different wave and wind conditions on the dynamics of the support structure. In this regard, the influence of the wind speed on the aerodynamic damping of the fundamental FA and side-side (SS) modes will be analyzed. The second part of this section compares the acceleration levels obtained from the model with the tuned damping and measurements. During the measurements, the ambient parameters are different at each measurement data point. Therefore, it is necessary to select the proper measurement data. For example, to study the effect of the wave period on the structure, the data is extracted for different wave periods while the other parameters, e.g., wind speed and wave height are kept constant. In the next section, we will compare the measured acceleration levels with the simulated data. Therefore, we will apply wind and wave loads to the tuned model.

5.1. Tuning the damping

Offshore support structures are stressed by several loads, especially if the excitation loads have frequencies that are close to the structure's eigenfrequencies. In general, the role of damping is to remove energy from a system by dissipation. This can be carried out internally and externally.

An externally introduced damping effect is caused by external forces affecting the dynamic system; examples are aerodynamic or hydrodynamic damping. Internal damping is related to the energy dissipation in the materials and is mainly introduced by material damping through internal friction. Also, in soil dynamics, the material damping enables energy dissipation by grain boundaries and microstructure defects.[27]

The overall damping of an offshore wind turbine support structures consists of the aerodynamic damping, damping due to constructive devices and additional damping, e.g., structural damping. The additional damping is influenced by further effects, e.g., soft soil and hydrodynamic damping.[28] Therefore, the overall measured system damping (D_{tot}) can be approximated as a linear combination of following damping sources:

$$D_{\text{tot}} = D_{\text{struc}} + D_{\text{soil}} + D_{\text{aero}} + D_{\text{hydro}} + D_{\text{mass.damp}} \tag{1}$$

with D_{struc} as the material damping of structure, D_{soil} as the soil damping due to inner soil friction, D_{aero} as the aerodynamic damping and $D_{\text{mass.damp}}$ as the tower TMD; $D_{\text{hydro}} = D_{\text{radiation}} + D_{\text{vis}}$ is the hydrodynamic damping, which consists of two terms; $D_{\text{radiation}}$ is the damping from wave creation due to structure vibration; D_{vis} is the viscous damping due to hydrodynamic drag.

It is the goal of this section to summarize how the overall damping in the model has been tuned in such a way that it corresponds well with the measurements. For this study, we study the overall damping of the first fundamental modes of the support structure in FA direction. In the work by Devriendt *et al.*,[24] the overall damping of the FA mode of the monitored wind turbine has been identified by performing an overspeed stop while the TMD was not active. A value of 1% damping was found. On the same day, several data-sets, while the wind turbine was parked with the TMD not active and with low wind speeds around 4 ms^{-1}, have been analyzed using operational modal analysis. Damping values for the FA mode varied between 0.8% and 1.2%. This corresponds well with the suggested values in the work by WindEnergie.[28] Devriendt *et al.*[13] discuss the results of the 2 weeks monitoring period for the same wind turbine in parked conditions while the TMD was active. The mean damping value of the FA mode for wind speeds between 0 and 6 ms^{-1} was found to be 1.7% (see Table V for wind speeds of 4–6 ms^{-1}). We can conclude that within these 2 weeks, the overall damping of the first FA mode was between 0.4% and 0.5% higher than the previous tests in parked conditions while the TMD was not active. Note that the measurements are only able to give values for the overall damping. It is impossible to identify the different damping contributions independently. We can, however, consider that during the aforementioned experiments, the aerodynamic damping was negligible in the FA direction, considering the parked conditions and the very low wind speeds.

The difficulty in the simulations is to select the different damping contributions in the model in such a way that the overall damping is in agreement with the measurements. Table IV lists the different damping contributions selected in the simulations based on the measurement results obtained from the overspeed stop. A detailed discussion on choosing and evaluating the damping factors is provided in the Shirzadeh *et al.*[14] To achieve the overall damping of, e.g., 1%, a

Table IV. An overview of the contribution of each source of damping in overall damping of the first FA mode.

Test case	D_{struct}	D_{soil}	D_{aero}	D_{hydro}	D_{tot}
Overspeed stop test (without TMD)	0.60	0.25	0.08	0.07	**1.0**
Parked WT- ambient excitations (with TMD)	1.20	0.20	0.17	0.12	**1.69**

Table V. Damping ratios (ζ) for the first FA and SS modes for different wind speed ranges obtained from measurements.

Wind speed range (ms^{-1})	S1FA mean damping ratio (ζ%)	S1SS mean damping ratio (ζ%)
4–6	1.73	2.18
6–8	1.79	2.76
8–10	1.92	2.72
10–12	2.10	2.81
12–14	2.20	3.18
14–16	2.17	2.97
16–18	2.77	3.19

starting value of 0.6% damping was selected as the structural damping. This value is based on engineering judgment and is in agreement with the reported measurement data.[29] It considers both the material damping of steel and the damping due to the internal joints and the grouted connection. The soil damping will be selected in such a way that the overall damping, including the hydrodynamic and aerodynamic damping, will result in a value of 1% when analyzing the time domain simulations using operational modal analysis. The actual soil damping can then simply be found by performing an eigenvalue analysis, as both the structural damping and soil damping are modeled as a Rayleigh type of damping. The contribution of the hydrodynamic damping can be evaluated by analyzing a time domain simulation while the aerodynamic loading calculation is set to off (this simulates the case by removing the wind loading). Finally, the aerodynamic damping can be identified by performing time domain simulations at corresponding wind speed. For the monitoring period while the TMD was active, an overall damping of 1.7% was found. So an additional 0.7% of damping needs to be added to the model in comparison with the overspeed stop. Here, we encounter the first important limitation of the used simulation software, e.g., we cannot include a localized damper just below the nacelle level to model the TMD. We decided to simply increase the Rayleigh damping of the supporting structure (monopile and tower). It was found that when the structural damping was increased from 0.6% to 1.20%, the overall damping in the time domain simulations would give a value around 1.69% for the overall damping, which is in agreement with the measurements. Table IV lists again the different damping contributions. Note that the increase of the structural damping changes all the damping contributions.

5.2. Effect of wind speed on the damping of fundamental FA and SS modes

The damping contribution that is mostly influenced by ambient conditions is the aerodynamic damping. Therefore, we will analyze the effect of wind speed on the damping values of the fundamental support structure modes in FA and SS directions. The wind turbine is again in parked condition, and the blades are pitched to 78°. Table V illustrates the damping ratios of the first FA and SS modes for different wind speed ranges obtained from the measurements.

The simulations have been performed at different wind speeds (from 4 up to 18 ms^{-1}), whereas the wind-wave misalignment is 20°. The damping values from simulations at wind speed of 4 ms^{-1} are in perfect agreement with the measurement data obtained during the short measurement campaign while the TMD was active, where we found 1.7% and 2.18% for, respectively, the first FA and SS modes. These results were expected as the simulations have been tuned to have a damping ratio of 1.69% for the first FA mode, as was discussed earlier. The damping values for different wind speeds have been estimated from simulations. The damping values of the FA and SS modes are compared with the measurements in Figure 7. The measurement damping estimations are provided as a box plot in which the center lines give the median value for estimates within a case. The outer lines of the box indicate the 25th and 75th percentile. Outliers are indicated with a + sign.

In both measurements and simulations, we find a slightly higher damping for the first SS mode (S1SS) in comparison with the first fore-aft mode (S1FA). This can be explained because of the presence of some extra aerodynamic damping effects in the SS direction considering the high pitch angle in parked conditions. According to Hansen *et al.*,[30] the aerodynamic forces are present even at the standstill because of the larger blade surface that interacts with surrounding air when the tower vibrates in the SS direction.

Wind Energ. 2015; **18**:1685–1702 © 2014 John Wiley & Sons, Ltd.
DOI: 10.1002/we

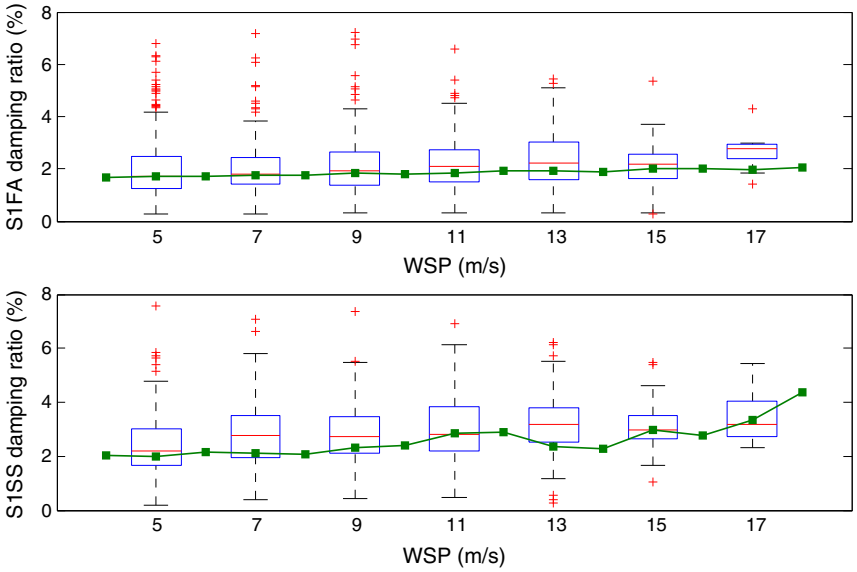

Figure 7. Damping values for the first FA and SS modes as a function of wind speed for a parked wind turbine. Blue boxes show the damping values for different wind speed bins from measurements data averaged for an interval of 2 ms^{-1}. The green solid lines show the simulated damping ratios from HAWC2.

Comparing the damping values between the low wind speed and the high wind speed, we notice an overall increase of the damping ratio for both FA and SS modes. This can be attributed to the higher drag forces at higher wind speeds, which would result in higher aerodynamic damping values. It can be concluded that for the S1FA mode, the mean damping values of measurements coincides very well with the damping values obtained from the simulations. This is not true for the wind speed between 16 and 18 ms^{-1}. In fact, the last wind-speed bin does not contain a lot of measurement data, and therefore, these results might be less reliable.

For the S1SS mode, the simulations seem to slightly underestimate the damping at certain wind speeds, especially at wind speed range of 13–15 ms^{-1}. One can also see from these figures that the relative increase of the damping value due to higher wind speeds in the SS direction is higher than in the FA direction. Therefore, we can conclude that for high wind speeds in parked conditions, the aerodynamic damping mechanism is dominant in the SS direction, whereas in the FA direction, the overall damping remains dominated by the additional offshore damping contributions such as the structural damping and soil damping. Note that up to now, we assume that, e.g., the soil damping remains constant even for high excitation levels. Future research intends to analyze at what extend the assumption that all other damping contributions can be considered as constant is valid. It might be expected that also soil damping is load dependent. Also, the TMD might be more effective at higher excitation levels.[9]

5.3. Comparison of acceleration levels

In the previous section, we discussed how we tuned the model to be in good agreement with the measurements. In this section, we will evaluate if this is sufficient for correctly predict the acceleration levels in various ambient conditions using the simulations. Therefore, the acceleration levels obtained from the measurements will be compared with those from simulations. The influence of wave period, wave height and wind speed will be analyzed.

First, the influence of the wave period and wave height on the response of the wind turbine is analyzed. The measurement data at Belwind revealed that during the short-term measurements, the wave period varied mainly between 3 and 5 s at the Belwind wind farm. The accelerations from simulations are captured at three levels while the wave period was altered between 2.5 and 5.2 s with an increment of 0.2 s. The root mean square (RMS) values of the accelerations at three levels in FA and SS directions are shown in Figure 8.

The acceleration levels have a clear peak around 2.8 s. This is expected considering the fact that the first bending mode of the tower is around 0.36 Hz or 2.86 s. Therefore, the waves have the possibility to excite the support structure into dynamically amplified vibrations, as the wave period gets closer to the fundamental foundation frequencies. For higher wave periods, the amplitude of the accelerations is reduced. Although the measurements show a similar trend, the amplitudes of measurement accelerations are much lower than those obtained by the simulations, especially in the FA

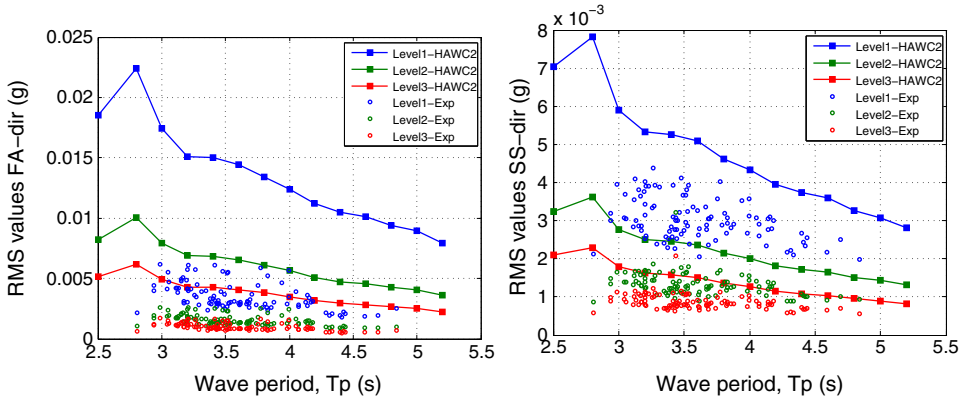

Figure 8. The RMS values of accelerations for different levels in FA (left) and SS (right) directions as a function of wave period. The measurement data points have been filtered such that WSP < 6 ms^{-1} and $0.4 < H_s < 0.6$ m.

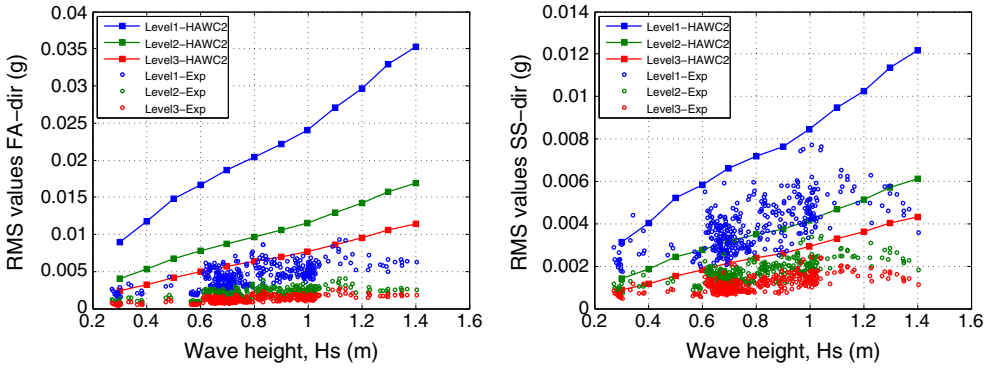

Figure 9. The RMS values of accelerations for different levels in FA (left) and SS (right) directions as a function of wave height. The measurement data points have been filtered such that WSP < 6 ms^{-1} and $3 < T_p < 3.8$ s.

direction. In general, we can say that the simulated vibration levels are between a factor of two and three times higher than measurements data.

Furthermore, the effect of the significant wave height on the acceleration levels is considered on the basis of the measurements in parked condition, where the wave height varied between 0.3 and 1.4 m. The measurements dataset is filtered for the wave periods between 3 and 3.8 s and low wind speed (WSP $<$ 6 ms^{-1}). A constant wave period 3.5 s is used for all simulations while the wave height is increased from 0.3 up to 1.4 m with an increment of 0.1 m. The acceleration levels versus wave height are demonstrated in Figure 9. The measurement data show an increase with the wave height. The simulation results reproduced the same behavior with the wave height. For the wave height larger than 1 m, the measured accelerations seem to stay more or less constant. In a similar way to the first analysis, the simulations overestimate the RMS values comparing with the measurements especially in the FA direction. Especially at the high wave heights, the simulations tend to overestimate the vibration levels up to a factor six.

In the last analysis, the effect of wind speed on the measured and simulated acceleration levels is considered. The acceleration levels for different wind speeds at FA and SS directions are displayed in Figure 10.

Looking into the acceleration levels in the FA direction, a small variation is observed with increasing the wind speed. This was expected as the blades are pitched, and the aerodynamic loading is negligible in this direction. It was previously concluded that the damping in the FA direction is dominated by the additional offshore damping even at higher wind speeds. In the SS direction, however, we can notice a small increase of RMS levels toward higher wind speeds.

The aforementioned analyses showed that RMS levels for both direction are still overestimated. This might suggest that the damping contributions have not been properly selected during the tuning procedure. This also can be the result of the uncertainty of input data in both wave and wind models. In the next section, we will perform a sensitivity analysis for the different parameters used in the simulations, and a discussion will be given to show the effect of the parameters on the vibration levels.

Wind Energ. 2015; **18**:1685–1702 © 2014 John Wiley & Sons, Ltd.
DOI: 10.1002/we

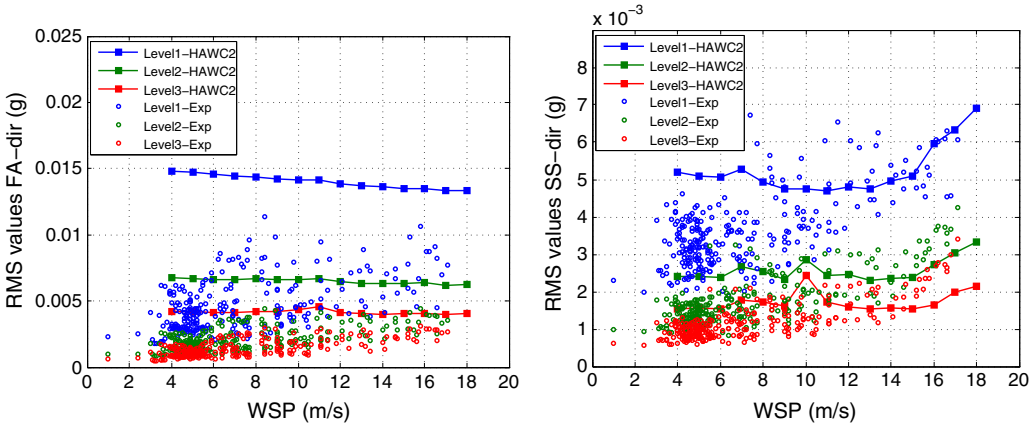

Figure 10. The RMS values of accelerations for different levels in FA (left) and SS (right) directions for different wind speeds. The measurement data points have been filtered such that $3 < T_p < 3.8$ s and $0.4 < H_s < 0.6$ m.

6. SENSITIVITY ANALYSIS OF THE WIND AND WAVE PARAMETERS

This section discusses the results of the sensitivity analysis for damping values, wind and wave parameters. All figures show the comparison of the top level acceleration. The reference case in the simulations is the point where $WSP = 4.5$ ms^{-1}, $H_s = 0.5$ m, $T_p = 3.5$ s and the overall damping value is 1.69% according to the Table IV.

6.1. Damping distribution

A possible reason for the overestimation might be that the damping is not properly selected during the tuning phase. From Table IV, it can be seen that the selected structural damping and soil damping were, respectively, 1.20% and 0.20%. In the next paragraph, we will study the effect of the damping values on the RMS levels using two sets of test cases.

For the first analysis, the summation of the soil and structural damping are kept constant around 1.40% while the contribution of each term is changing. The overall damping of the S1FA mode is calculated in time domain analysis. Although the summation of structural and soil damping values remains constant, the overall damping is larger for the cases with higher soil contribution (Table VI). The soil damping is increased from 0.20% to 0.94% as the structural damping is reduced from 1.2% to 0.46%. Figure 11 shows the top-level RMS values for different damping contributions in FA and SS directions. As a result, because of the increase in the total damping, the RMS values are decreased. However, the RMS values predicted by the simulations remain larger than the measurements. An increase of about 1.17% in the overall damping value has been resulted to a reduction of 20% in the vibrations levels in FA direction. Although the RMS values can be reduced for higher damping values, the higher damping values are not realistic based on the measurement results.

Table VI. Soil and structural damping values for different cases.

Test case		Structural damp (%)	Soil damp (%)	Total damp (%) Eigenvalue	Total damp (%) Time domain
Constant structural and soil damping	Case 1	1.20	0.20	**1.40**	1.69
	Case 2	1.03	0.37	**1.40**	2.00
	Case 3	0.94	0.45	**1.40**	2.15
	Case 4	0.46	0.94	**1.40**	2.86
Constant overall damping	Case 1	1.20	0.20	1.40	**1.69**
	Case 2	1.03	0.24	1.27	**1.69**
	Case 3	0.94	0.26	1.20	**1.68**
	Case 4	0.46	0.40	0.86	**1.68**

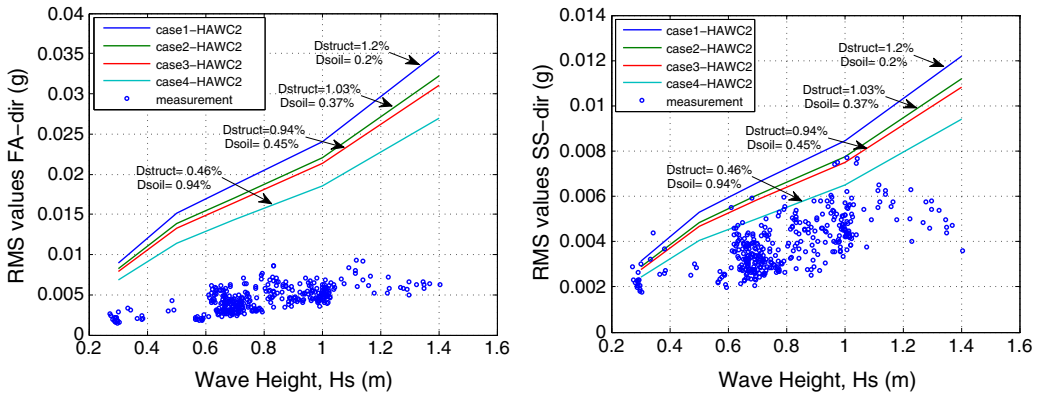

Figure 11. The RMS values of accelerations at top-level in FA direction (left) and SS direction (right) for different combinations of structural and soil damping while their sum is kept constant. The measurement data points have been filtered such that WSP $<$ 6 ms^{-1} and $3 < T_p < 3.8$ s.

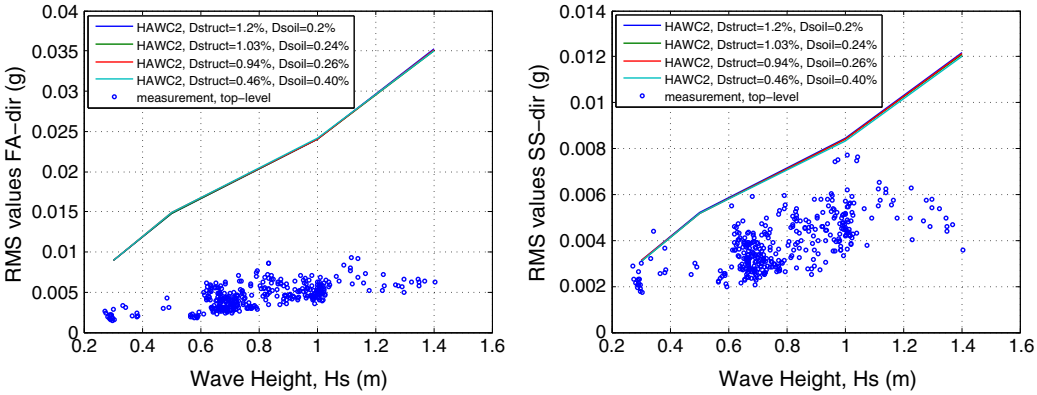

Figure 12. The RMS values of accelerations at top-level in FA direction (left) and SS direction (right) for different combinations of structural and soil damping while the overall damping is kept constant. The measurement data points have been filtered such that WSP $<$ 6 ms^{-1} and $3 < T_p < 3.8$ s.

During the second analysis, the overall damping of the S1FA mode is constant in all cases. The soil and structural contributions have been chosen in such a way that the overall damping in time domain is around 1.69%. Table VI shows the cases with different soil and structural damping contributions where the overall damping is kept constant. The simulations are repeated again for different wave heights. Figure 12 compares the top-level acceleration in FA and SS directions for different test cases. The RMS values for all cases are near identical. It can be concluded that as long as the overall damping is constant, the RMS values will not be affected by the different damping contributions.

Here, again, we see that the simulations keep overestimating the acceleration levels for all combinations of soil and structural damping.

6.2. Sensitivity to the wind speed

In Section 5.3, it was shown that the RMS values stayed nearly constant for the wind speed ranged between 4 and 12 ms^{-1}. To study the effect of wind loading on the vibration levels, a sensitivity analysis is performed for different wind speeds. The simulations are carried out at different wind speeds, and the RMS values of the top level are compared with the reference case. In addition to the wind speed, the effect of turbulence is determined by performing a case with laminar flow. Figure 13 shows that the RMS values are loosely dependent on the wind speeds. The RMS values in the SS direction however are more sensitive to the wind speed as the blades are pitched in parked conditions. This proves our previous discussion that the influence of the wind loads on the RMS values are negligible in parked conditions.

Wind Energ. 2015; **18**:1685–1702 © 2014 John Wiley & Sons, Ltd.
DOI: 10.1002/we

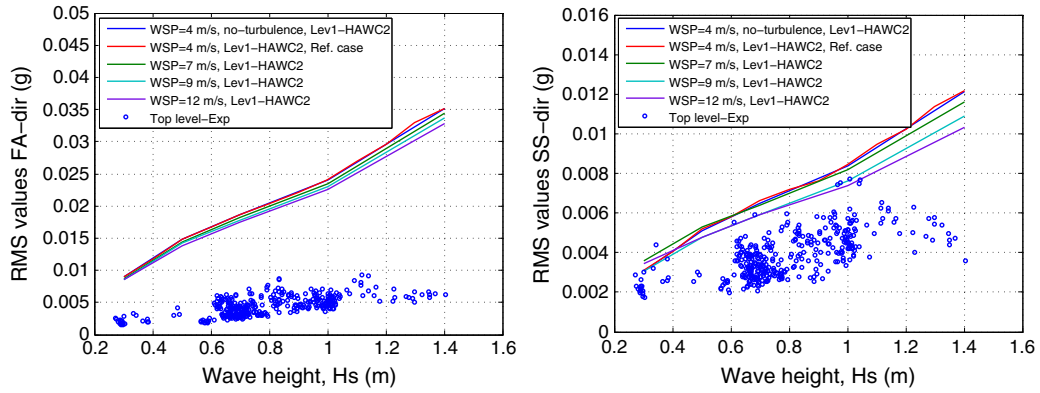

Figure 13. The RMS values of accelerations at top-level in FA direction (left) and SS direction (right) for different wind speeds. The measurement data points have been filtered such that WSP < 6 ms^{-1} and $3 < T_p < 3.8$ s.

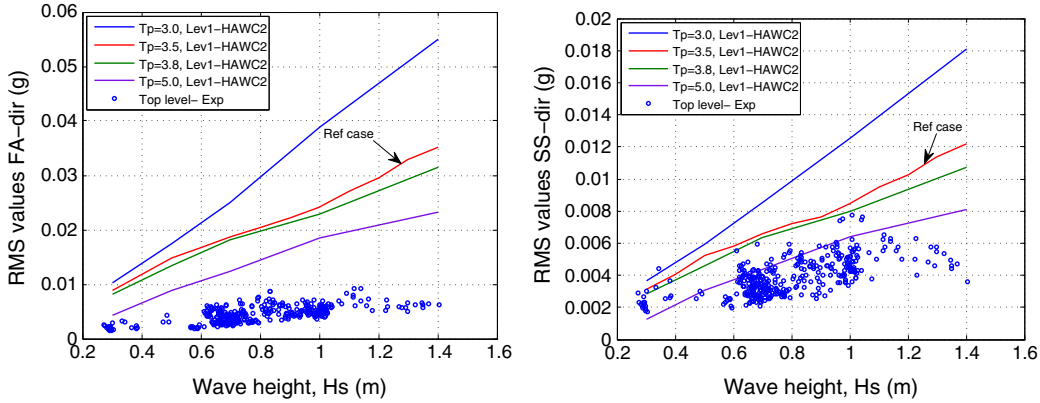

Figure 14. The RMS values of accelerations at top-level in FA direction (left) and SS direction (right) for different wave periods. The measurement data points have been filtered such that WSP < 6 ms^{-1} and $3 < T_p < 3.8$ s.

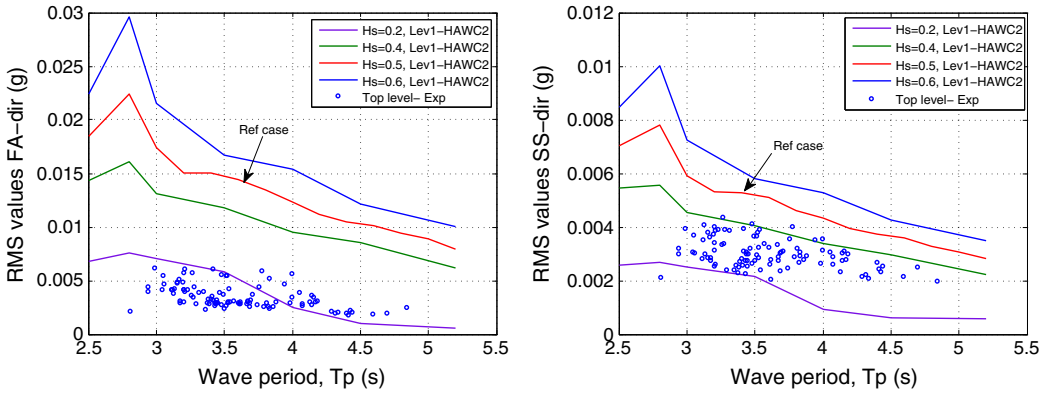

Figure 15. The RMS values of accelerations at top-level in FA direction (left) and SS direction (right) for different wave heights. The measurement data points have been filtered such that WSP < 6 ms^{-1} and $0.4 < H_s < 0.6$ m.

6.3. Sensitivity to the peak period of the wave

The RMS levels as a function of wave height are illustrated in Figure 14 for different wave periods. Because the measurements are filtered for $3 < T_p < 3.8$ s, we also did the simulations with the same filtering limits. In contrast with the wind

speed, the wave period has a significant impact on the RMS levels. For the case with $T_p = 3$ s, the vibrations are intensified because the wave period is getting closer to the frequency of the first FA mode. Simulations continue to be high even for the highest wave period of 3.8 ms^{-1}.

6.4. Sensitivity to the significant height of the wave

Figure 15 represents the variation of the RMS values versus wave period for different wave heights. It is clear that the vibrations are getting larger for higher wave heights. The simulations are also performed for the boundaries of the measurement filtering.

The wave load is definitely the most dominant load, and as shown in the aforementioned sensitivity analysis, the wave parameters have the largest influence on the RMS levels of the vibrations of the wind turbine in parked conditions.

7. CONCLUSION

This paper studies the dynamics of an offshore V90 3MW wind turbine installed at Belwind wind farm. The structural properties of wind turbine and its support structure as well as the wave kinematics, wind conditions and soil parameters are implemented in HAWC2. The natural frequencies of the structure identified from eigenvalue analysis and time domain simulations in HAWC2 are then compared with measurements. Both simulations and measurement results are processed using a state-of-the-art operational modal analysis technique, pLSCF. The resonance frequencies obtained from the simulations show a satisfactory agreement with the measurement results.

The overall damping of the first FA mode has been estimated from both overspeed stop test and ambient excitations measurements.[24] The overall damping of the model was tuned to be in agreement with the measurements. The tuning procedure has been discussed in this paper. Using the updated model, the influence of different wave and wind parameters on the dynamic response of the wind turbine has been studied. We have analyzed the simulated acceleration levels for different parameters, e.g., wave period, wave height and wind speed. The overall trend of the simulations and measurements was in good agreement. However, the simulations seemed to overestimate the vibration levels.

Therefore, it was concluded that although the model was well modeled on the basis of the exact design parameters and according to the existing standards and that the dynamic parameters such as frequencies and damping values were in good agreement with the measurements, the simulations did not correctly predict the acceleration levels. It is obvious that this can have important consequences on the correct calculation of the fatigue life of an offshore wind turbine. A detailed sensitivity analysis is carried out for both damping values and wave-wind parameters.

It is shown that the wave parameters and thus wave loads have the largest influence on the vibration levels. The difference between the measurements and simulations is likely found in the simulated wave loads. As we discussed earlier, the Morrison's equation is not valid for the large diameter piles ($D/L < 0.2$). This can cause an overestimation of the wave loads due to the higher C_m values. Diffraction theory should be employed to correct the inertia coefficient for large diameters. However, there is little empirical validation of this correction in the real-life conditions, and it remains a potential cause of the difference between the simulations and measurements. Therefore, the calculation of wave loads in simulations and validation thereof is a topic that requires further research. Other smaller differences can also be attributed to the fact that the used wave parameters are not exactly representing the wave conditions at the wind turbine locations. For this reason, we currently extended the measurement campaign with a wave-radar at the turbine location.

ACKNOWLEDGEMENTS

The research presented in this paper is conducted in the framework of the 'Offshore Wind Infrastructure Application Lab' www.owi-lab.be. The authors gratefully thank the people of Belwind NV for their support before, during and after the installation of the measurement equipment.

REFERENCES

1. The european offshore wind industry—key trends and statistics 2013, *Technical Report*, The European Wind Energy Association (EWEA), January 2014. [Online]. Available: http://www.ewea.org/ (Accessed on April 2014).
2. Pure power ii: wind energy targets for 2020 and 2030, *Technical Report*, The European Wind Energy Association (EWEA), 2011. [Online]. Available: http://www.ewea.org/ (Accessed on April 2014).

3. Madariaga A, de Alegría IM, Martín J, Eguía P, Ceballos S. Current facts about offshore wind farms. *Renewable and Sustainable Energy Reviews* 2012; **16**(5): 3105–3116.
4. Philippe M, Babarit A, Ferrant P. Modes of response of an offshore wind turbine with directional wind and waves. *Renewable Energy* Jan 2013; **49**(SI): 151–155, DOI: 10.1016/j.renene.2012.01.042. 11th World Renewable Energy Congress and Exhibition, Abu Dhabi, U Arab Emirates, Sep 25-30, 2010.
5. Petersen B, Pollack M, Connell B, Greeley D, Davis D, Slavik C, Goldman B, Medley L. *Evaluate the effect of turbine period of vibration requirements on structural design parameters: technical report of findings*, 2010.
6. Tarp-Johansen NJ, Energy D. Comparing sources of damping of cross-wind motion. *European Offshore Wind Conference (EOW). DONG energy*, Stockholm, Sweden, 2009.
7. Van Der Tempel J. Design of support structures for offshore wind turbines, *Ph.D. Thesis*, Technical University of Delft, 2006.
8. Larsen TJ, Madsen HA, Larsen GC, Hansen KS. Validation of the dynamic wake meander model for loads and power production in the Egmond aan Zee wind farm. *Wind Energy* 2013; **16**(4): 605–624.
9. Damgaard M, Ibsen LB, Andersen LV, Andersen JKF. Cross-wind modal properties of offshore wind turbines identified by full scale testing. *Journal of Wind Engineering and Industrial Aerodynamics* 2013; **116**: 94–108.
10. Häckell MW, Rolfes R. Monitoring a 5 MW offshore wind energy converter—Condition parameters and triangulation based extraction of modal parameters. *Mechanical Systems and Signal Processing* 2013; **40**(1): 322–343.
11. Ozbek M, Rixen DJ. Operational modal analysis of a 2.5 MW wind turbine using optical measurement techniques and strain gauges. *Wind Energy* 2013; **16**(3): 367–381.
12. Devriendt C, Jordaens PJ, De Sitter G, Guillaume P. Damping estimation of an offshore wind turbine on a monopile foundation. *EWEA 2012*, Copenhagen, Denmark, 2012.
13. Devriendt C, Jordaens PJ, Van Ingelgem Y, De Sitter G, Guillaume P. Monitoring of resonant frequencies and damping values of an offshore wind turbine on a monopole foundation. *EWEA 2013 Conference*, Vienna, Austria, 2012.
14. Shirzadeh R, Devriendt C, Bidakhvidi M, Guillaume P. Experimental and computational damping estimation of an offshore wind turbine on a monopile foundation. *Journal of Wind Engineering and Industrial Aerodynamics* 2013; **120**(0): 96–106, DOI: http://dx.doi.org/10.1016/j.jweia.2013.07.004.
15. Chauhan S, Hansen M, Tcherniak D. Application of operational modal analysis and blind source separation/independent component analysis techniques to wind turbines. *Proceedings of XXVII International Modal Analysis Conference*, Orlando (FL), USA, 2009.
16. Veldkamp H, Van Der Tempel J. Influence of wave modelling on the prediction of fatigue for offshore wind turbines. *Wind Energy* 2005; **8**(1): 49–65.
17. Din E. 19902: 2008-07: Petroleum and natural gas industries-fixed steel offshore structures (iso 19902: 2007). *English version EN ISO 2007;* 19902.
18. Najafian G, Tickell R, Burrows R, Bishop J. The UK Christchurch Bay compliant cylinder project: analysis and interpretation of morison wave force and response data. *Applied Ocean Research* 2000; **22**(3): 129–153.
19. Veritas DN. *DN-OS-J101 design of offshore wind turbine structures,* DNV, September 2011.
20. Hasselmann K, Barnett T, Bouws E, Carlson H, Cartwright D, Enke K, Ewing J, Gienapp H, Hasselmann D, Kruseman P, Meerburg A, Muller P, Olbers DJ, Richter K, Shell W, Walden H. Measurements of wind-wave growth and swell decay during the joint north sea wave project (JONSWAP), 1973.
21. Jonkman J, Butterfield S, Musial W, Scott G. Definition of a 5-MW reference wind turbine for offshore system development, National Renewable Energy Laboratory, 2009.
22. Institute AP. Recommended practice for planning, designing, and constructing fixed offshore platforms-working stress design: upstream segment. *API recommended practice 2A-WSD (RP 2A-WSD). API*, 2000.
23. Passon P. Memorandum: derivation and description of the soil-pile-interaction models. *IEA-Annex XXIIII Subtask* 2006; **2**.
24. Devriendt C, El-Kafafy M, De Sitter G, Guillaume P. Estimating damping of an offshore wind turbine using an overspeed stop and ambient excitation. *15th International Conference on Experimental Mechanics, ICEM15*, Porto, Portugal, 2012.
25. Peeters B, Van der Auweraer H, Guillaume P, Leuridan J. The polymax frequency-domain method: a new standard for modal parameter estimation? *Shock and Vibration* 2004; **11**(3–4): 395–410.
26. Maia NMM, Silva JMM. *Theoretical and experimental modal analysis*, 1997.

27. Fischer T, de Vries W. Final report task 4.1, deliverable d 4.1.5 (wp4: offshore foundations and support structures), project upwind eu project no. 019945 (ses6) integrated wind turbine design.
28. WindEnergie GL. Guidelines for the certification of offshore wind turbines, 2004, Final Draft, Edition.
29. Veritas DN. *Guidelines for design of wind turbines,* DNV, 2009.
30. Hansen M, Thomsen K, Fuglsang P, Knudsen T. Two methods for estimating aeroelastic damping of operational wind turbine modes from experiments. *Wind Energy* 2006; **9**(1–2): 179–191.

Wind Energ. 2015; **18**:1685–1702 © 2014 John Wiley & Sons, Ltd.
DOI: 10.1002/we